Bio-inspired mechanisms for inclined locomotion in a legged insect-scale robot

Benedikt F. Seitz*, Benjamin Goldberg*, Neel Doshi*, Onur Ozcan*, David L. Christensen†, Elliot W. Hawkes†, Mark R. Cutkosky†, and Robert J. Wood*

***Abstract*—Legged locomotion is an open problem in robotics, particularly for non-level surfaces. With decreasing robot size, different issues for climbing mechanisms and their attachment and detachment appear due to the physics of scaling. This paper describes micro-scale phenomena for different adhesion methods that can be employed in microrobots. These adhesion methods are applied to a sub-2 gram legged robot, the Harvard Ambulatory MicroRobot (HAMR), by leveraging recent advances in milli- and micrometer-scale manufacturing. The presented designs utilize different passively oriented adhesives on the legs of the robot to improve inclined locomotion performance. A 3DoF ankle joint is designed and implemented and the effects of a passive tail are studied. As a result, HAMR's climbing capability is increased from 3^o inclines to 22^o inclines and 45^o declines. Finally, an analytical model of leg and foot force generation is presented and compared with experimental force data from the attachment mechanism on a single-leg experimental setup.**

I. Introduction

Over the last decade, bio-inspired legged robots have become increasingly agile. By adapting principles and mechanisms of legged-locomotion found in nature, high performance robots with characteristic dimensions in the range of 0.2-0.5 meters are able to walk, run [1], jump [2], climb [3] and even swim [4]. Engineers are now moving towards the design and fabrication of robots at the insect scale. Recent advances in fabrication methods, control mechanisms, and actuator designs have led to robots with millimeter and centimeter scale features such as HAMR [5], [6] and DASH [7]. Currently, locomotion for HAMR has been demonstrated only on level, flat surfaces. Improving the agility and flexibility of these insect scale robots with the addition of adhesion and climbing mechanisms will lead to new directions of research and bolster insect scale robot performance in applications such as search and rescue, surveillance, and inspection, as well as biological research.

Current insect-scale legged robots have explored obstacle traversal [8] but have not been designed for locomotion on inclined or inverted surfaces. At larger scales, climbing mechanisms and adhesion technologies for robots around 0.2-1 meter in characteristic length have been designed and implemented with sophisticated attachment and detachment mechanisms [9]. Despite the challenges in scaling down these mechanisms, we hypothesize that a decrease in scale will allow the climbing mechanisms to benefit from an increase in the surface area to volume ratio.

Adhesion methods used in climbing robots include *electroadhesion*, *micro-spine adhesion* and *gecko-like dry adhesion*. *Electroadhesion* uses an electrostatic force to create normal adhesion between an electrode and a polarizable surface [10]. By appropriate patterning of the electrode, a shear force can also be induced. *Micro-spine adhesion* uses surface asperities to create a high friction force and an adhesion force normal to the surface. On rough surfaces artificial micro-spine adhesives can endure loads of 70 grams and more per spine [11]. *Gecko-like dry adhesives* use micron-size features to create Van der Waals forces that induce normal adhesion. By orienting the features in a single direction, a predetermined attachment and detachment direction can be chosen [12]. The asymmetry of these features encourages the adhesive to attach when applying a shear force parallel to the climbing surface that engages the features and increases the area of contact [13].

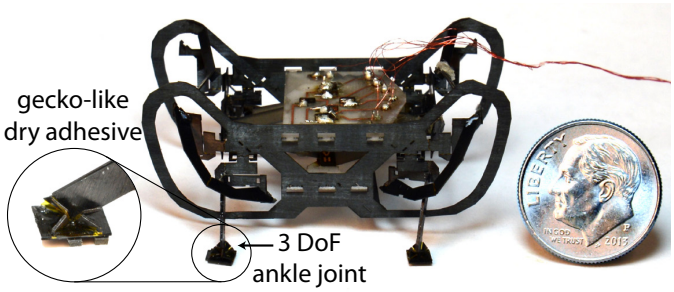

Fig. 1. Harvard Ambulatory MicroRobot with a 3DoF ankle joint and gecko-like dry adhesive.

Applying any of these adhesion methods requires sufficient alignment between the adhesive material and surface. At larger scales, small misalignments lead to catastrophic failures as the contact area is reduced drastically. This has led to robot designs that include precise attachment and detachment processes [3]. At the micro-scale the effects of misalignments are reduced, making less complex attachment processes possible. However, such attachment and detachment mechanisms are still necessary in order to ensure that a minimum contact area is maintained. We propose the use of a passively aligned foot to achieve the level of alignment necessary for an insect scale robot. Finally, to design a passive foot, the locomotion characteristics of the robot have to be known, and these characteristics are presented for HAMR. The resulting robot outfitted with this passively oriented ankle mechanism and gecko-like dry adhesive is shown in figure 1.

II. Adhesion models

This paper considers electroadhesion, micro-spine adhesion and gecko-like dry adhesion, implemented on HAMR as a representative insect-scale robot.

*Harvard Microrobotics Laboratory, Harvard University, Cambridge, Massachusetts 02138, USA. Email: see http://www.micro.seas.harvard.edu

†Biomimetics and Dexterous Manipulation Lab, Stanford University, Stanford, California 94305, USA. Email: see http://bdml.stanford.edu

A. Electroadhesion

A charged plate, isolated by a dielectric material and in contact with a polarizable surface, induces a surface charge. The resultant electrostatic force attracts (or repels) the plate to (or from) the surface via the following equation:

$$F = A\epsilon_d\epsilon_v \frac{\Delta V^2}{2d^2}, \tag{1}$$

Here d is the thickness of the insulator, A is the area of the electrode, ϵ_v and ϵ_d are the dielectric permittivity of vacuum and the insulator, respectively, and ΔV is the applied voltage. Implementing a pattern of alternating positively and negatively charged electrodes (figure 2) has the advantage of also inducing a secondary shear force.

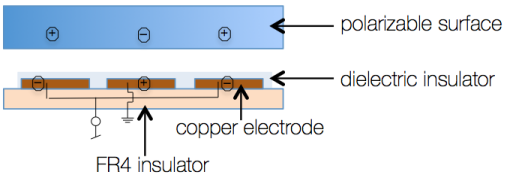

Fig. 2. Interaction between a charged electrode array and polarisable surface.

The electro adhesives, shown in figure 3 are fabricated using a dry-etch laser ablation process with a diode-pumped solid state (DPSS) laser where the desired electrode pattern is etched into a $1/2$ $oz.$, 0.005" thick copper-clad FR-4 board. A $15\mu m$ parylene dielectric layer is deposited in a vacuum deposition chamber. This process enables conformal coatings of uniform controllable thickness.

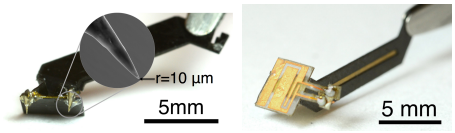

Fig. 3. Mounted micro-spine adhesive (*left*) and mounted electroadhesive (*right*).

B. Gecko-like dry adhesives

Artificial gecko adhesives try to imitate the adhesive performance of gecko feet, which show a non-adhesive state unless pre loaded with shear to engage with a surface [14]. The performance of gecko feet, and thus the performance of artificial dry adhesives, is modeled by *Frictional Adhesion*, a model that is illustrated by a two dimensional limit curve. The force space limit curve defines the stable area, where combinations of normal force and shear force represent stable contact between the adhesive and the climbing surface. Generally, higher shear forces allow for higher normal forces. Furthermore, the origin is on the boundary on this limit curve, implying that for zero shear force a non-adhesive state is possible, requiring zero normal force for detachment [15].

The friction force is rooted in Van der Waals interactions of the micro-features with the surface. The induced friction force per feature is a function of contact area:

$$F_{fric}[L(U)] = \mu \cdot \underbrace{(b \cdot L(U) \cdot \overbrace{\frac{A}{6 \cdot \pi \cdot D^3}}^{\textit{van der Waals contact pressure}})}_{\textit{induced normal adhesive force}}, \tag{2}$$

The contact area, defined by $L(U)$, is a function of the bending energy of the feature. The Frisch-Fay model describes the bending strain energy as:

$$U = \int_0^L \frac{EI(s)}{2}\left(\frac{d\phi}{ds}\right)^2 ds, \tag{3}$$

where s is the arc-length, ϕ is the tangent angle along the beam length, E is the elastic modulus, and I is the moment of inertia [16].

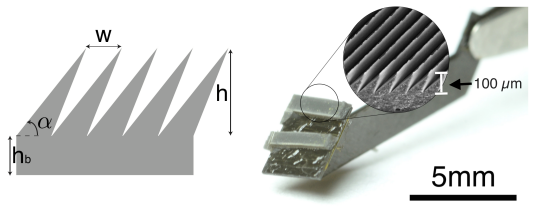

Fig. 4. Gecko-like dry adhesive model *(left)*, mounted dry adhesive *(right)*.

The artificial dry adhesive, shown in figure 4, consists of an array of wedge shaped polymer features [$50\mu m \leq h \leq 200\mu m$, $20\mu m \leq w \leq 70\mu m$] and a thin backing layer [$50\mu m \leq h_b \leq 100\mu m$] that are fabricated in a molding process. The mold is fabricated using a CNC-micromachining process. Polydimethylsiloxane is then applied to the mold and cured at 21^{o}C for 24 hours [12].

C. Micro-Spines

Recent advances in micro-scale fabrication have made the implementation of micro-spines possible. The small feature size of the spine generates normal adhesion forces on rough surfaces. The spines use surface asperities to create a primary shear force and a secondary normal force. The adhesion mechanism and the introduction of primary and secondary forces is shown in figure 5 along with a limit curve to visualize the attachment process.

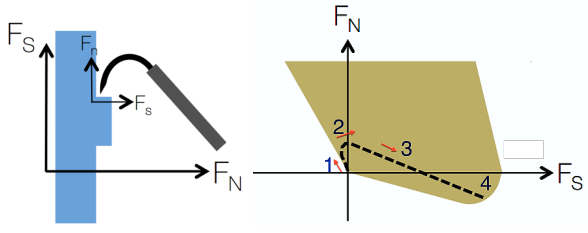

Fig. 5. Normal and shear forces acting on a microspine *(left)* and limit curve displaying an optimal attachment trajectory *(right)*.

The limit curve in figure 5 can also be used to visualize the necessary loading trajectory. Starting at the origin (1), the first

contact with the surface shows a positive normal force (2). Moving the spine parallel to the surface increases the shear force (3) and the achievable negative normal force (normal adhesive force) increases (4). The performance is limited by the tensile strength of the asperity and micro-spine [11].

To create microspines, two *Daiichi Premium Fishing Hooks*™ with $r = 10\mu m$ tip radius are mechanically fixed on HAMR legs at 90^o, perpendicular to the coronal plane of the robot as shown in figure 3.

III. Harvard Ambulatory MicroRobot

The adhesion mechanisms described in section II are explored on an insect-scale quadrupedal robot, HAMR. This section gives an overview of the robot and relevant locomotion performance characteristics, and presents an alignment mechanism to ensure proper contact is made between the adhesion mechanism and climbing surface.

A. Fabrication and actuator performance

The fabrication process used to make HAMR is the Printed Circuit Microelectromechanical Systems (PC-MEMS) process. This utilizes pop-up assembly to unfold a multilayer laminate into fully articulated 3D structure as described in [6]. The robot transmission employs a flexure-based spherical five-bar hip joint driven by externally powered, optimal energy density, piezoelectric bending bimorph actuators [17]. The actuator and transmission forces were measured to determined the effect of the transmission on climbing performance. Figure 6 shows the experimental setup for the characterization of a single actuator.

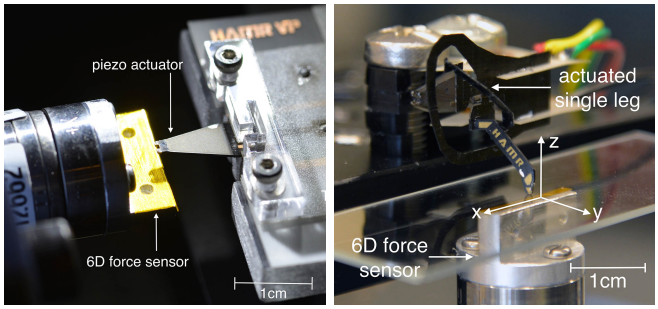

Fig. 6. Single actuator and single-leg test platform with actuator fixture and Nano17 Titanium six axis force/torque sensor.

Several actuator versions are available as discussed in [18]. The difference between actuators are in the thickness of the central conducting carbon fiber layer. The pre-stacked, 2-ply actuators used in HAMR display a maximum peak-to-peak free deflection of $400\mu m$ and a maximum single-sided blocked force of $250mN$, measured empirically on the setup shown in Figure 6. Furthermore, the pre-stacked 2-ply actuators have the greatest mechanical energy and thus were chosen over 3-ply, 1-ply and non-pre-stacked actuators, which were eliminated due to their limited range of motion or limited force output.

Secondly, the transmission performance was quantified in a single-leg experimental setup. A complete HAMR and a single leg, shown in figure 6, were fixed on a force platform and the walking gait was simulated. Measuring the force output at the end of the leg and comparing it with the actuator force as a function of input voltage allows us to quantify the performance of the flexure-based spherical five bar hip joint. At a control signal amplitude and frequency (200V, 0.5Hz) the transmitted force is measured to be 5.5 (mN), showing that energy is lost in the transmission. Including the theoretical transmission ratio ($R_{TR} = \frac{InputForce}{OutputForce} = \frac{20}{1}$) based on transmission linkage lengths of HAMR, an efficiency factor Q_{trans} was determined as follows:

$$Q_{trans} = \frac{F_{max,out}}{F_{max,in} \cdot R_{TR}} \approx 58\% \tag{4}$$

B. Locomotion characteristics

The robot uses a trot gait due to the coupling of the actuators described in [5]. Since this gait only has two legs touching the ground at any time, the robot does not have a tripod of stability during the gait which results in a rocking motion. This motion, detrimental to climbing ability, was recorded and the roll and pitch angles were calculated. The rocking motion of HAMR shows roll angles of 0.15 radians and pitch angles of 0.25 radians as shown in figure 7. On inclines, the pitch angle increases due to gravitationally induced torque.

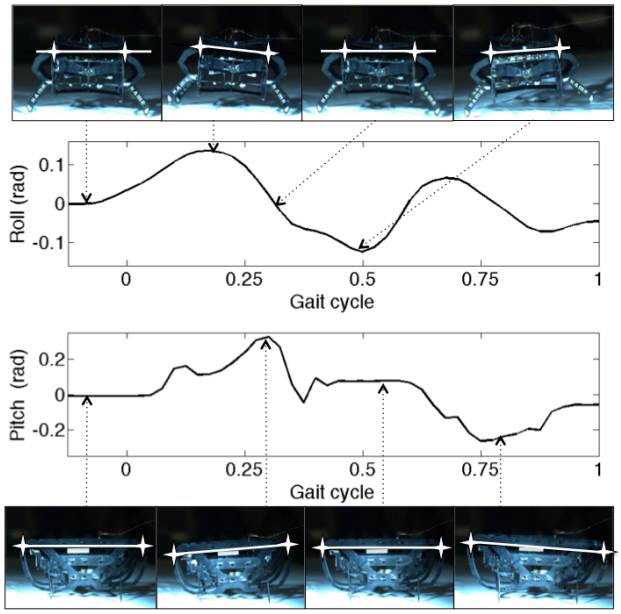

Fig. 7. Roll and pitch angles, quantified by 3D image processing for a full locomotion cycle on a non-inclined surface.

Finally, the trajectory of HAMR's leg has not been optimized for climbing purposes. The lift actuator drives the leg in an arc in the z (*vertical*) and y (*transverse*) directions. The swing actuator drives the leg in an arc that is predominantly in the x (*sagittal*) direction. Combining these motions with a 90 degree phase offset causes the tip of the leg to move in a diagonal ellipse. Ground contact alters the trajectory as the leg is fixed to climbing surface for negative z-values, causing the trajectory to look more like a half-ellipse. Further analyzing the trajectory of the leg shows that during surface contact the greatest amplitude is in the y-direction, which is perpendicular to the both the direction of locomotion, x, and lift, z.

C. Design adaptations

The roll angle and pitch angles during the gait cycle can be reduced by implementing a passive tail (shown in figure 8a) and thus providing the necessary tripod of stability [19]. A $5cm$ long tail has a mass of $120mg$ and is fabricated from five strands of 33AWG wire. The spring-like tip has an approximate stiffness of $15N/m$ which passively controls the induced normal force and thus the counter torque. Reduced rocking motions enable better alignment of the adhesive materials and thus better locomotion performance of the robot.

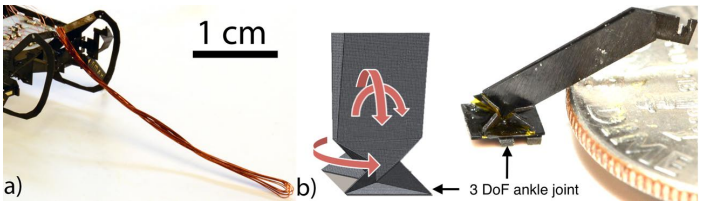

Fig. 8. a) Passive tail b) Five-bar ankle joint model (*left*), and final version with adhesive(*right*).

D. Implementation of adhesives

The locomotion characteristics indicate that a passive 3DoF joint must be implemented to provide sufficient alignment. Roll and pitch angles exceed 0.17 radians during walking and may lead to detachment due to a misalignment of the adhesives. Thus, we designed a passive five-bar ankle joint (shown in figure 8b) and manufactured it using the PC-MEMS fabrication paradigm. The ankle was designed to enable self alignment of the foot for a normal force of $2mN$, less than one-quarter of HAMR's weight. This was achieved with a torsional spring of $k \approx 12 \cdot mN/rad$. Using the 3 DoF joint, HAMR is capable of self-aligning the adhesion mechanisms during the walking gait and provides an even mounting surface for the adhesives.

IV. Experiments and Results

Different adhesives were fabricated and their performance on HAMR was recorded. The shear and normal adhesion forces have been recorded on the single leg setup and walking tests on inclined and declined surfaces have been conducted.

A. Single leg forces

On the single leg setup, HAMR was loaded with 0.7g (equal to half the body weight) and the actuators were activated with the standard gait control signal amplitude and frequency (200V, 0.5Hz) to simulate walking. The experiments included three trials with seven cycles each. The peak shear force data and peak normal adhesive force data was recorded for a single trial after eliminating the first and last cycle.

1) Electro Adhesion: Three example cycles of the shear and normal forces for electroadhesives with a surface area of $9.25mm^2$, parylene dielectric thickness of $15\mu m$ and an excitation voltage of 1000V are shown in figure 9. The average peak shear force for electroadhesion on a glass surface increases from $2.2mN$ to $5.5mN$ with the voltage off and on, respectively. The detachment force (normal adhesion force) for the electro adhesives is $4.1mN$.

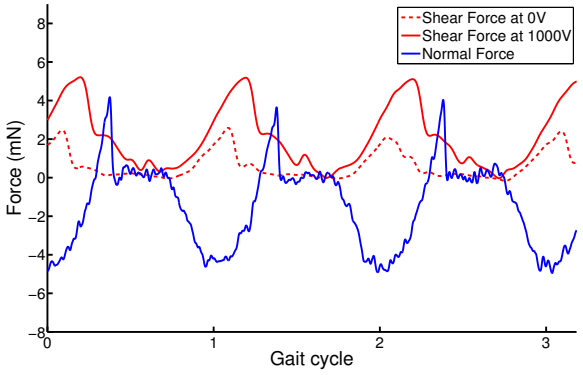

Fig. 9. Shear force (in the x-direction) and normal force (in the z-direction) for electroadhesives over three cycles on a single leg setup.

2) Dry Adhesion: Three different artificial gecko adhesives were tested on a glass surface:

1) Non-directional wedges, w=60μm, h=100μm with a total area of $8mm^2$
2) Directional wedges, w=60μm, h=100μm, α_{tilt}=60^o with a total area of $8mm^2$
3) Directional wedges, w=30μm, h=50μm, α_{tilt}=60^o with a total area of $8mm^2$

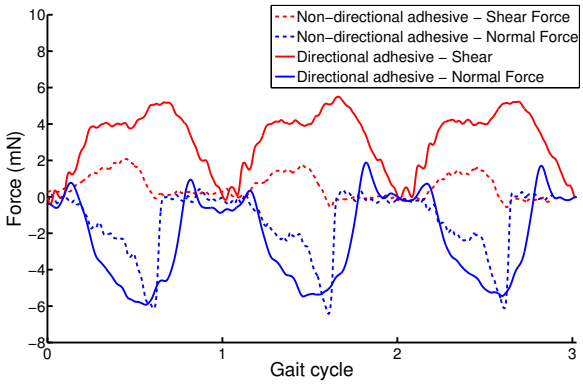

Fig. 10. Shear force (in the x-direction) and normal force (in the z-direction) for directional and non-directional adhesives ($h = 100\mu m$) over three cycles on a single leg setup.

Three example cycles of the shear and normal force for directional and non-directional adhesives are shown in figure 10. A negative normal force in these plots is the preload force that represents the body weight of HAMR ($\sim 6mN$). The average peak shear force of directional adhesives with $h = 100\mu m$ and $h = 50\mu m$ (not shown) yield similar values of $F_S = 5.5mN$. The shear force for non-directional adhesives ($F_S = 2mN$) is reduced in comparison to directional adhesives. Normal adhesion for the directional adhesives is approximately 80% reduced for features with $h = 50\mu m$ compared to features with $h = 100\mu m$ ($F_N = 2mN$). Non-directional adhesives show a negligible normal force of ($F_N = 0.15mN$).

3) Micro-spine Adhesion: The orientation of the micro-spine adhesives is perpendicular to the surface due to limited

control over the leg trajectories. Detachment of angled spines is only possible for leg trajectories that include a retrieving stroke in the locomotion direction. For HAMR angled spines are thus not capable of producing the desired adhesion forces. Perpendicular spines do not cause a normal adhesion and inclines above 15^o are therefore not feasible. On a single leg setup, the maximum shear force on a cardstock surface caused by the micro-spines is $5.1mN$. A summary of the average peak normal and shear force over all trials for each of the described attachment mechanisms is shown in figure 11.

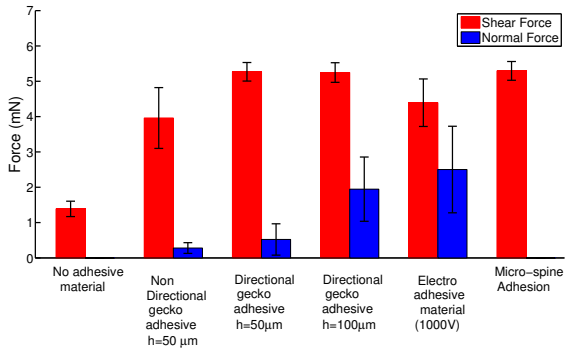

Fig. 11. Normal force and shear force of different adhesive materials with standard deviation of 21 data points.

B. Climbing test

The performance of each adhesive was then tested by integrating them on HAMR and evaluating climbing on inclined surfaces (the angle of the surface relative to the horizontal is defined as γ as shown in figure 12). Dry adhesives and electro adhesives were tested on a smooth glass surface, micro-spine adhesives were tested on cardstock with surface roughness k $\approx 2 \cdot 10^{-4}m$.

Inclined locomotion with electroadhesive materials is not possible for inclines with an angle $\gamma > 10^o$. The synchronisation of leg movement and electrode charging is critical and the alignment between the foot and the ground is not sufficient. The adhesive fails to provide sufficient shear and normal force, causing the feet to slip.

Inclined locomotion with artificial dry adhesives is possible for inclines of $\gamma < 22^o$. Locomotion on declined surfaces was possible for $\gamma \leq 45^o$ without slipping. Alignment is sufficient and slipping does not occur on inclines of $\gamma \leq 45^o$.

Inclined locomotion with micro-spine feet is possible on inclines of $\gamma > 12^o$. Locomotion on declined surfaces was possible for $\gamma \leq 15^o$ without slipping. Due to the limited leg trajectory, an adhesion force can not be induced. For higher inclines, the orientation of the spines has to be optimized, requiring the trajectory to be altered. A summary of the incline and decline climbing performance is shown in figure 13.

V. Discussion and Conclusion

This study shows a novel approach to inclined locomotion for legged robots at the insect scale. Recent advances in micro-fabrication are leveraged to adapt a variety of adhesive materials to an existing locomotion mechanism instead of

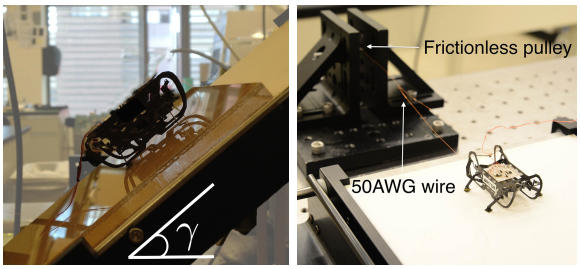

Fig. 12. Climbing test on a 45^o inclined glass surface with gecko-like dry adhesive *(left)* and towing test on a cardstock surface with 250mg towing load *(right)*.

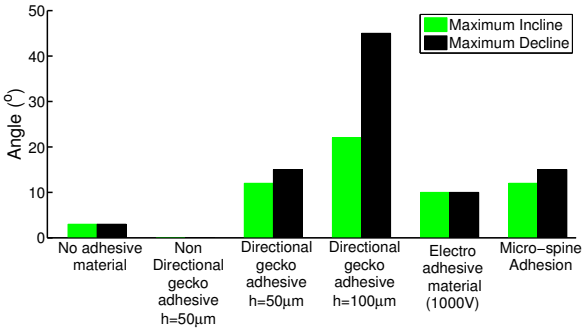

Fig. 13. Succesful locomotion on different inclines and declines.

adapting a locomotion mechanism to an adhesive material. The variety of available adhesion mechanisms will also enable hybrid solutions, which will be investigated in future work. An example of a hybrid micro-spine and dry adhesive system

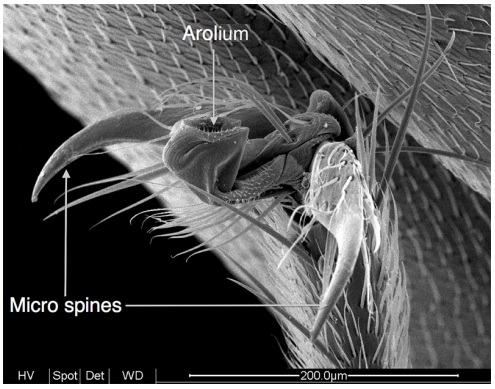

Fig. 14. Hybrid foot of a *Oecophylla smaragdina* ant, including micro-spines and soft Arolium [*courtesy of C. Castro*].

found in nature is shown in figure 14 and discussed in [20]. Future work will explore similar hybrid systems in HAMR. For example, combinations of dry adhesives and electroadhesives may benefit from a positive feedback loop. The normal force, induced by the electroadhesives may help in aligning the dry adhesive. Better alignment of the dry adhesive will lead to a larger contact area and thus greater adhesion. This again decreases the distance between the electrode and the surface and increases the effects of the electroadhesives [13]. *Spenko and Parness* recently showed that a hybrid adhesive increases the adhesion performance of dry adhesives up to 510%. It

was also shown that the adhesion is dependent on the surface roughness and the surface material. For rough surfaces the hybrid adhesive creates a higher adhesion than the sum of single electroadhesives and dry adhesives [13].

We showed that milli-and micro-scale robots profit from reduced misalignment difficulties and that dry adhesives and micro-spine adhesive provide sufficient shear force to overcome inclined surfaces. With the implementation of a passive, ankled foot and a passive tail, the effects of induced torque and induced rocking motions are compensated.

The analytical models show that HAMR fails to climb higher inclines due to power limitations and not due to shear force limitations of the adhesive materials. Verified by single leg force measurements, the adhesives are capable of withstanding shear loads of 1.1g, equivalent to the induced shear load of HAMR on a 66^o inclined surface. The work showed that the actual robot performance does not reach the limitations suggested by the models, likely due to transmission losses, perturbations from missteps, or miss synchronization of feet touchdown or pull off. Towing experiments, shown in figure 12, confirmed that the compliance within the transmission also has the effect of reducing the stride length as the shear load due to gravity increases with the angle of the incline. Future work will include the optimization of the robot performance by increasing the force output and the stride length.

When optimizing and orienting the adhesive material, the attachment direction is equal to the direction of the longest leg stride during touchdown. For HAMR the longest stride is in *coronal plane* and *transversal plane*, meaning in the y-direction perpendicular to the locomotion direction. The experiments showed the highest locomotion performance when the directional dry adhesives were oriented with asymmetry in the y-direction.

Finally, this work shows that legged locomotion at insect scales favor six legged locomotion. By including two additional legs the available power increases linearly. In contrary to increasing the size of the actuators, the power-to-weight ratio will stay constant when including more actuators, as growing in a single direction increases the surface area for adhesion and the weight linearly. Furthermore, redundancy is increased, stability is increased, and the ability to bridge gaps is greater.

VI. Acknowledgment

The authors thank Dr Carlos Castro and Dr James Weaver for providing the SEM images. This work is partially supported by the National Science Foundation (award numbers CMMI-1251729 and DGE-1144152), the Army Research Laboratory (award number W911NF-08-2-0004), and the Wyss Institute for Biologically Inspired Engineering. Any opinions, findings, and conclusions or recommendations expressed in this material are those of the authors and do not necessarily reflect the views of the National Science Foundation.

References

[1] J. E. Clark. *Design, simulation, and stability of a hexapedal running robot*. PhD thesis, Stanford University, 2004.

[2] X. Zhou and S. Bi. A survey of bio-inspired compliant legged robot designs. *Bioinspiration & biomimetics*, 7(4):041001, 2012.

[3] M. F. Silva, J. Machado, and J. K. Tar. A survey of technologies for climbing robots adhesion to surfaces. In *Computational Cybernetics, 2008. ICCC 2008. IEEE International Conference on*, pages 127–132. IEEE, 2008.

[4] G. Dudek, M. Jenkin, C. Prahacs, A. Hogue, J. Sattar, P. Giguere, A. German, H. Liu, S. Saunderson, A. Ripsman, et al. A visually guided swimming robot. In *Intelligent Robots and Systems, 2005.(IROS 2005). 2005 IEEE/RSJ International Conference on*, pages 3604–3609. IEEE, 2005.

[5] A. T. Baisch, O. Ozcan, B. Goldberg, D. Ithier, and R. J. Wood. High speed locomotion for a quadrupedal microrobot. *The International Journal of Robotics Research*, doi:0278364914521473, 2014.

[6] A. T. Baisch and R. J. Wood. Design and fabrication of the harvard ambulatory micro-robot. In *Robotics Research*, pages 715–730. Springer, 2011.

[7] P. Birkmeyer, K. Peterson, and R. S. Fearing. Dash: A dynamic 16g hexapedal robot. In *Intelligent Robots and Systems, 2009. IROS 2009. IEEE/RSJ International Conference on*, pages 2683–2689. IEEE, 2009.

[8] K. L. Hoffman and R. J. Wood. Robustness of centipede-inspired millirobot locomotion to leg failures. In *Intelligent Robots and Systems (IROS), 2013 IEEE/RSJ International Conference on*, pages 1472–1479. IEEE, 2013.

[9] A. T. Asbeck, S. Kim, A. McClung, A. Parness, and M. R. Cutkosky. Climbing walls with microspines. In *Proc. of the 2006 IEEE International Conference on Robotics & Automation*, pages 4315–4317, 2006.

[10] H. Prahlad, R. Pelrine, S. Stanford, J. Marlow, and R. Kornbluh. Electroadhesive robots—wall climbing robots enabled by a novel, robust, and electrically controllable adhesion technology. In *Robotics and Automation, 2008. ICRA 2008. IEEE International Conference on*, pages 3028–3033. IEEE, 2008.

[11] A. T. Asbeck and M. R. Cutkosky. Designing compliant spine mechanisms for climbing. *Journal of Mechanisms and Robotics*, 4(3):031007, 2012.

[12] P. Day, E. V. Eason, N. Esparza, D. Christensen, and M. Cutkosky. Microwedge machining for the manufacture of directional dry adhesives. *Journal of Micro and Nano-Manufacturing*, 1(1):011001, 2013.

[13] A. Parness, T. Hilgendorf, P. Daniel, M. Frost, V. White, and B. Kennedy. Controllable on-off adhesion for earth orbit grappling applications. In *Aerospace Conference, 2013 IEEE*, pages 1–11. IEEE, 2013.

[14] B. Bhushan and R. A. Sayer. Gecko feet: natural attachment systems for smart adhesion. In *Applied Scanning Probe Methods VII*, pages 41–76. Springer, 2007.

[15] E. W. Hawkes, J. Ulmen, N. Esparza, and M. R. Cutkosky. Scaling walls: Applying dry adhesives to the real world. In *Intelligent Robots and Systems (IROS), 2011 IEEE/RSJ International Conference on*, pages 5100–5106. IEEE, 2011.

[16] N. Esparza *Design of bio-inspired directional tapered adhesives and hierarchies*. PhD thesis, Stanford University, 2012.

[17] R.J. Wood, E. Steltz, and R. Fearing. Optimal energy density piezoelectric bending actuators. *Sensors and Actuators A: Physical*, 119(2):476–488, 2005.

[18] O. Ozcan, A. T. Baisch, D. Ithier, and R. J. Wood. Powertrain selection for a biologically-inspired miniature quadruped robot. In *IEEE Intl. Conf. on Robotics and Automation, Hong Kong, China*, May 2014.

[19] M. H. Dickinson, C. T. Farley, R. J. Full, M. Koehl, R. Kram, and S. Lehman. How animals move: an integrative view. *Science*, 288(5463):100–106, 2000.

[20] W. Federle and T. Endlein. Locomotion and adhesion: dynamic control of adhesive surface contact in ants. *Arthropod Structure & Development*, 33(1):67–75, 2004.